Chapter 3
Molecular Motors: Cooperative Phenomena of Multiple Molecular Motors

Stefan Klumpp, Corina Keller, Florian Berger and Reinhard Lipowsky

Abstract Transport of various types of cargoes in cells is based on molecular motors moving along the cytoskeleton. Often, these motors work in teams rather than as isolated molecules. This chapter discusses analytical and computational approaches to study the cooperation of multiple molecular motors theoretically. In particular, we focus on stochastic methods on various levels of coarse-graining and discuss how the parameters in a mesoscopic theoretical description can be determined by averaging of the underlying microscopic processes. These methods are applied toward understanding the effects of elastic coupling in a motor pair and in the cooperation of several motors pulling a bead. In addition, we review how coupling can have different effects on different motor species.

3.1 Background

Long-distance transport in cells is powered by molecular motors of the kinesin, myosin, and dynein superfamilies that move along microtubules or actin filaments [41, 64, 81]. Representatives of each superfamily have been characterized biochemically, structurally, and biophysically in some detail. In particular, the development of single-molecule techniques has greatly expanded our knowledge about the dynamics of these motors and provided a detailed picture of the stepping of the motors and the forces they exert [19, 42, 70, 82, 86, 89, 97]. These experimental efforts have been complemented by theoretical investigations studying relatively coarse-grained stochastic descriptions of one or several chemomechanical working cycles of specific molecular motors [12, 29, 44, 61]. In addition, molecular dynamics and Brownian dynamics simulations, using both detailed empirical force fields as well as structure-based (Gō-type) approaches, have been used to address the mechanical details of the motors' molecular motion, see, e.g., [33, 43, 45].

S. Klumpp (✉) · C. Keller · F. Berger · R. Lipowsky
Max Planck Institute of Colloids and Interfaces, Science Park Golm,
14424 Potsdam, Germany
e-mail: klumpp@mpikg.mpg.de

S. De et al. (eds.), *Multiscale Modeling in Biomechanics and Mechanobiology*, DOI 10.1007/978-1-4471-6599-6_3

In cells, these motors often work in small teams rather than as single molecules [9, 34]. Therefore in recent years, the cooperation of motors and the dynamics of motor complexes have moved to center stage, in experimental [5, 22, 34] as well as theoretical studies [9, 51]. In contrast to earlier work on motor cooperation [46], which mostly dealt with large numbers of motors, as in the contraction of muscle, which is based on the cooperation of billions of myosin molecules [40], the recent studies focus on defined complexes of small numbers of motors, starting with motor pairs up to complexes of 7 motors. These numbers are typical for transport in cells, as indicated by electron microscopy and as deduced from *in vivo* force and velocity measurements [34].

Specifically, the recent development of synthetic complexes linking a defined number of motors [1, 25, 30, 66, 79, 96] enables the detailed quantitative characterization of the dynamical behavior of coupled motors using the techniques originally developed for single motor molecules. Previous quantitative characterizations of coupled motors [5, 90] have remained somewhat limited by the fact that only the average number of motors rather than their actual number could be prescribed. These synthetic complexes link motors via a DNA linker [30, 66, 79], a quantum dot [1], an antibody [96], or via a DNA origami scaffold [25]. In particular, the latter method allows to control the numbers and types of motors as well as their geometric arrangement.

In this chapter, we discuss the analytical and computational treatment of cooperative molecular motors and motor complexes consisting of a small number of motors coupled with elastic linkers. We review three approaches describing such systems at different levels of detail, with different theoretical scopes and invoking different computational costs. The three approaches start with different descriptions of single motor molecules, specifically (i) as a random walker on a chemomechanical network of motor conformations, (ii) as a stochastic stepper with force-dependent rates, and (iii) as a molecule moving in three spatial dimensions subject to geometric constraints such as binding to a bead, but with a rather coarse-grained description of its internal degrees of freedom. In all three cases, we consider two or more such motors coupled via some elastic element, which may correspond to the flexible stalk or tail of the motor, a linker molecule, or the common cargo of the coupled molecular motors.

3.1.1 Length and Time Scales of Molecular Motor Motility

The movements of individual motor molecules as well as of motor complexes involve motion on a wide range of length scales, which we illustrate here for the best studied motor, dimeric kinesin-1 (conventional kinesin). The movement of kinesin-1 (as well as of other cytoskeletal motors) is powered by the hydrolysis of adenosine triphosphate (ATP) to adenosine diphosphate (ADP). The kinesin-1 dimer has two heads, each of which contains an ATP binding site and can bind to a microtubule. The hydrolysis reaction involves conformational rearrangements in the ATP binding pocket that occur on a length scale of $\lesssim$1 nm. These small movements lead

to allosteric conformational changes in other parts of the same head of the motor, including the microtubule binding site. They also affect the other head, possibly via the generation and release of strain between the two heads [35, 45, 76, 99]. This process is believed to involve the docking of a flexible structure called the neck linker to the leading head [76] and ultimately leads to large-scale motion of the rear head, the actual step of the motor.

That step, which brings the rear head of the motor in front of the leading head in a hand-over-hand fashion [100], is quite long, 16 nm for kinesin (and even 72 nm for myosin-V). The corresponding movements of the motor's center of mass is 8 nm (or 36 nm, respectively). Typically a single motor performs tens or even hundreds such steps while bound to the filament along which it walks, so that overall the motion of a motor bound to a filament proceeds over distances of $\sim 1\,\mu$m. This distance, which is called the run length and which is still quite small on the scale of the cell, is further increased by the cooperation of motors: Complexes with several motors can remain attached to a filament as long as at least one motor is bound to the filament, thus giving unbound motors a chance to rebind while the complex is still attached to the filament [51]. In addition to enhancing the overall run length of motors, motor cooperation also has an impact on the smaller length scales. In particular, the elastic coupling of the motors results in forces between the motors that can affect stepping, binding to the microtubule, and, via the motors' chemomechanical coupling, even their chemical rates of nucleotide binding and hydrolysis.

The corresponding timescales also range over several orders of magnitude. The transitions between different conformations of a single motor occur in the range of μs – s. Somewhat unexpectedly, the actual mechanical step is quite rapid with a rate of $\sim 10^5\,\mathrm{s}^{-1}$. The corresponding movement of a motor head over 16 nm happens instantaneously on the timescale of the experimental resolution of about 30 μs [19] (see also the discussion in Ref. [15]). By contrast, the chemical transitions, which correspond to much smaller spatial reorientations, are slower with rates of $\sim 0.01\ \mathrm{s}^{-1}$ (see the set of rates collected in [48, 61]). The entire chemomechanical cycle takes on average 0.01 s at saturating ATP concentrations, corresponding to a motor velocity of 800 nm/s in the absence of a load force. Unbinding of a kinesin motor from a microtubule occurs on a timescale of two orders of magnitude larger (~ 1 s), corresponding to a run length of $\sim 1\,\mu$m. For several motors, unbinding of motors is more frequent because all bound motors can unbind, so that the timescale of unbinding becomes smaller (and less separated from the stepping timescale). At the same time, unbinding of the cargo or the motor complex from the microtubule occurs on a longer timescale, as it requires unbinding of all motors. Estimates based on noninteracting motors lead to run times of many seconds or more. On such long timescales, additional effects become important, for example, the architecture of the cytoskeletal networks, because motors will often reach the end of a filament or filament–filament intersections. Using arrays of parallel isopolar microtubules large cargo particles have been shown to reach run lengths of millimeters, corresponding to runtimes of ~ 10 min [16].

3.2 Multiscale Computational Challenges

As discussed above, the dynamics of molecular motors and motor complexes involves movements on many different time and length scales. Therefore, typically different theoretical descriptions of the motors are used to study different aspects of their motility, dependent on the length and timescales on which the pertinent movements occur. The movements of molecular motors and motor complexes is often described using sets of discrete configurations or motor states, which may represent, for example, the chemical states of a motor or different mechanical configurations. Throughout most of this chapter we will follow the same strategy and describe systems of coupled motors by networks of discrete states and stochastic transitions between them. Such networks can however be constructed at many different levels of detail and we describe three of these below.

A key issue for the function of molecular motors is the coupling of mechanics and chemistry. At the level of a single motor, chemical (free) energy is converted into movement and work by the main chemomechanical cycle, in which hydrolysis of ATP in a motor head is followed by a mechanical movement of a motor head. An opposing load force can slow down the movement of the head, but may also induce backward steps and, via deformation of the motor head, affect the kinetics of the chemical processes such as ATP hydrolysis or ADP and phosphate release. In both cases, thermodynamic consistency imposes certain constraints relating the force-dependence of a rate to the force-dependence of the rate of the reverse process [61, 65]. The details of the chemomechanical cycle have consequences even on the largest time and length scales: Because the unbinding rate of a motor is dependent on its chemical state, changes in the nucleotide concentrations can modulate not only the motor velocity, but also the unbinding rate, and thus the run length. In a two-motor complex, such a modulation can shift the dominant mode of transport from a situation where transport is predominantly by a single motor bound to one where transport is predominantly by two motors [8, 96].

Specific to motor complexes is the question of coupling effects: If two or more motors are working cooperatively, will each of these motors work with the same characteristics as a single motor on its own or do motors interfere with each other? One generic reason for interference are forces between the motors that build up due to stochastic stepping: If coupled motors do not step in a synchronous fashion, the distance between the motors fluctuates over time and the linkers between the motors get stretched, thus mediating a fluctuating elastic force between the motors. If coupled motors interfere with each other, the next question is in what way do they interfere? Force between the motors may result in reduced stepping rates and thus a slow-down of the motor complex. In addition, however, a load force affects the unbinding rate of a motor, and thus its run lengths. Typically, the unbinding rate increases strongly with increasing force. As a consequence, a force between coupled motors could increase their unbinding rates and thus reduce the benefit of longer binding times (or run lengths) obtained from using several motors instead of just one. Indeed, both effects have been observed, with enhanced unbinding for a synthetic two-kinesin-1

motor complex [79] and reduced speed for a complex of two myosin V motors [66]. Reduced velocity has also been observed in microtubule gliding assays at high motor density with certain kinesin constructs with reduced flexibility [11, 24].

Our recent analysis of such interference effects has indicated the importance of the dynamic nature of these forces [7, 8]: Typically a motor will bind to the filament in a force-free fashion. The force between the motors is then built up by the stochastic stepping. The generation of forces of the order of the stall force (where a motor stops to step) or of the detachment force (the characteristic force scale for the unbinding rate) thus occurs over some characteristic timescales. These timescales have to be compared to the timescale for spontaneous unbinding, which provides a measure for the time the motors have to build up strain. If the time for spontaneous unbinding is very small, typically motors unbind before substantial strain is generated and thus interference effects are rather weak. A related issue arises when an external force is applied to a multi-motor complex: Only motors bound to the filament experience the load. When an additional motor binds to the filament, it will initially not experience any force and thus it will take some time until the force is actually shared equally among the bound motors. Equal force sharing is only reached if unbinding of motors is slower than the characteristic timescale for the equilibration of force sharing. Another question related to the stochastic stepping of the motors concerns the size of the observed steps. If the motors do not move in a synchronised fashion, steps that correspond to fractions of the single-motor step can be expected. This has indeed been observed in gliding assays for two motors, but not for three motors [58]. This observation has been attributed to nonequal force sharing between three motors [58] and to nonlinear elastic coupling between the motors [60].

Yet another longstanding challenge is the question how force is actually exerted on the molecules. This question is directly related to the spatial structure of the molecule. Force is typically exerted via the tail domain of the motor and somehow transmitted to the nucleotide binding pocket and to the microtubule binding site. How this force transmission occurs is not very clear. Important questions in this context are: Does the force experienced by the nucleotide binding pocket depend on the direction of the force in three dimensions? Is the commonly used one-dimensional description by a force along the direction of motion reasonably accurate? If not, which direction of force is characteristic in multi-motor complexes?

We conclude this section on the challenges to modeling and computation by a few general remarks. One rationale for using a palette of models at different scales, each appropriate for certain research questions, rather than a single model that describes everything, is the maxim attributed to Einstein to make things as simple as possible, but not simpler.[1] Doing so allows one to identify the key ingredients for certain phenomena to arise, while still being able to make quantitative predictions. This does not mean that further simplifications are useless. Further simplification may still be of use to provide a theoretical perspective on the core mechanisms. Nevertheless, one needs to keep in mind that every theoretical description is based on certain

[1] A discussion of the origin of the quote can be found at http://quoteinvestigator.com/2011/05/13/einstein-simple/#more-2363.

assumptions (which may be explicit or implicit) and should thus be expected to have a limited range of applicability. Outside this range its predictions may not be very reliable. As a matter of course, the construction of the model requires a careful choice of ingredients: Some results will not really be predictions, but rather rephrased statements of features of the model, as they have (explicitly or implicitly) been built into the model by way of its construction.

3.3 Methods

In the following we describe methods that have recently been developed for the theoretical and computational study of coupled molecular motors. We start with chemomechanical networks (Sect. 3.3.1) which provide a systematic framework for the description of individual motors that has very recently been extended to coupled motors [49]. We then discuss stochastic stepper approaches that are more coarse-grained in the sense that different chemical states of an individual motor are not distinguished and that movement is described by one or two effective stepping rates for forward and, possibly, backward steps (Sect. 3.3.2). The latter description can be further coarse-grained by characterizing the movement of a cargo by a set of velocities for different numbers of bound motors and not accounting for the individual steps of the motors. Finally, we briefly discuss approaches that describe the geometry of the motors and the cargo in some detail (Sect. 3.3.3). We conclude the discussion of the different methods with some general remarks and some comments on how the different methods can be integrated.

3.3.1 Chemomechanical Networks

A detailed description of single molecular motors is given by chemomechanical networks [61], which provide a generalization of simple enzymatic cycles. The use of networks rather than a single chemomechanical cycle is necessary to account for complex coupling between ATP hydrolysis and stepping [20, 44, 61]. For example, backward steps of kinesin-1 under superstall forces have been observed to require ATP, indicating that ATP is hydrolyzed rather than synthesized during the backward stepping cycle [19, 20]. As a consequence, the backward stepping cycle is different from the forward stepping cycle run in reverse. The chemomechanical network approach explicitly incorporates the chemistry behind the stepping process, i.e., the different chemical configuration of the motor domains. This theoretical framework has been used successfully for a quantitative description of experimental observations for kinesin-1 [48, 49, 61] and myosin V motors [12, 13].

Cargo transport by a motor complex or a small team of motors (that may belong to the same or to different motor species) can also be studied with chemomechanical networks. Each motor of such a team can be described by its chemomechanical

network which contributes to the team network. Moreover, each motor in the team has a finite run length, after which it dissociates from the filament. As long as the cargo is still connected to the filament by the remaining motors, the inactive motor has a chance to rebind to the filament. As a consequence, the number of actively pulling motors fluctuates. In the following, we focus on two identical motors, using two coupled kinesin-1 motors as an example [49].

3.3.1.1 Single Motor Network

The movement of a molecular motor on the filament is determined by the chemical reaction taking place within the catalytic domains of the motor which is coupled to a conformational change in the motor domains that causes translational motion of the motor. The dynamics of a molecular motor is described by a continuous-time Markov process on a discrete state-space or network [61, 65], the vertices of which represent the different chemical states of the two motor heads. The edges describe transitions between these states based on the network theory in enzyme kinetics introduced in [37]. The states of such a network are governed by certain dwell times that are exponentially distributed in a continuous-time Markov process [88]. The average dwell time in a certain state is given by the inverse of the sum of all transitions rates out of this state. The probability to find the motor in a certain state of such a network at a certain time is determined by the Master equation [88]. Our approach is based on identifying distinct motor states via the nucleotide occupancy of the two motor heads and (chemical as well as mechanical) stochastic transitions between these states.

The catalytic domain of each of the two motor heads of kinesin-1 can attain three different chemical configurations corresponding to the ATP-hydrolysis reaction: The binding pocket can be empty (E) or it can be occupied by ATP (T), by the cleavage products of the hydrolysis, ADP and phosphate (θ), or, upon phosphate release, by ADP alone (D). This classification thus leads to four different chemical states. Combining the cleavage transition ($T \rightarrow \theta$) and the phosphate release transition ($\theta \rightarrow D$) into a single transition ($T \rightarrow D$), one obtains a reduced network in which a single motor head can attain the three states E, T, and D. These states are linked by six transitions, each of which corresponds to binding or release of certain nucleotides as shown in Fig. 3.1a.

The two-headed kinesin motor can then attain $3^2 = 9$ states, but not all of these states are relevant to describe the dynamics of kinesin motors as shown in [61]. Two of these states, namely (EE) and (TT), should not play any prominent role in the processive motion of kinesin because the motor head is strongly bound to the filament when the head is empty or contains ATP, whereas it is only loosely bound to the filament when it contains ADP [80]. As a consequence, the motor most likely dissociates from the (DD) state. Neglecting the strongly bound states leads to the 7-state network shown in Fig. 3.1b.

Kinesin motors move in a hand-over-hand fashion [100] which implies that a mechanical step requires the interchange of the positions of the leading and trailing head of the motor. In principle, there are several possibilities to fullfill this condition

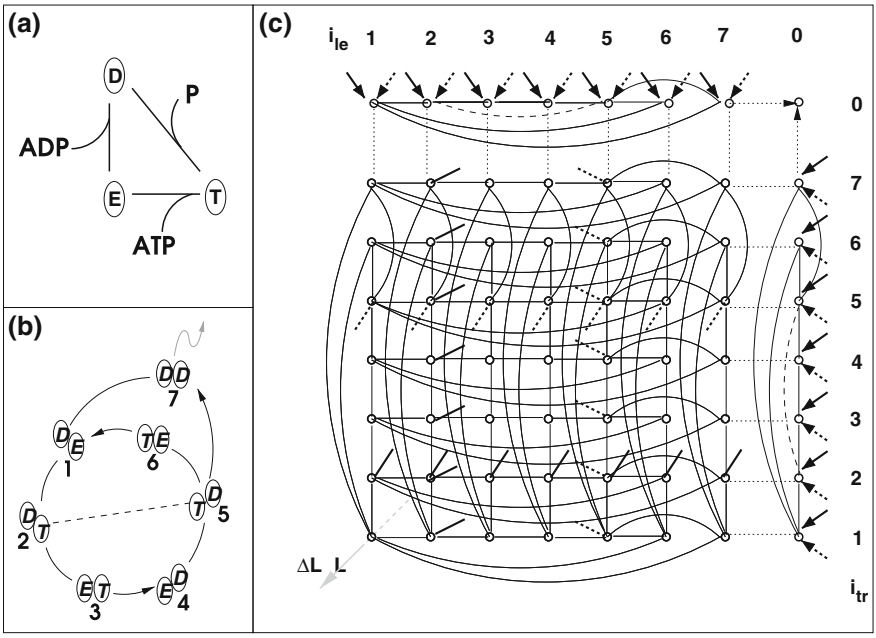

Fig. 3.1 **a** Kinetic diagram of a single motor head, for which hydrolysis and phosphate release have been combined into a single transition. **b** Chemomechanical 7-state network of the kinesin-1 motor as introduced in [61]. The *dashed line* represents the mechanical step, the *black arrows* indicate the direction of the ATP hydrolysis and the *gray arrow* indicates dissociation. Figure adopted from Ref. [61]. **c** State-space of motor pair as described by three coordinates [49]: the motor states $i_{\rm le}$ and $i_{\rm tr}$ of the leading and the trailing motor, and the extension ΔL of the elastic spring (axis perpendicular to the plane of the figure). In general, the motor pair states form a stack of layers, each of which corresponds to a fixed value of ΔL. Here, only the layer with $\Delta L = 0$ is shown. Open *circles* represent motor pair states, *thin lines* represent the chemical transitions between these states and *dashed lines* mechanical transitions during 1-motor runs. The thick stubs represent transitions to a neighboring ΔL-layer. Full stubs correspond to forward steps and broken stubs describe backward steps of one of the motors. *Dotted lines* represent binding and unbinding events between the single motor states $i = 7$ and $i = 0$, the latter describes an inactive motor. The *black arrows* indicate unbinding events emanating from any other ΔL-layer

for mechanical stepping, see Fig. 3.1b. The transition from (DT) to (TD) is taken to be the mechanical stepping transition [65], in agreement with single motor data.[2] The transition rates between two states i and j depend on the molar nucleotide concentrations $[X]$, with $X =$ ATP, ADP or P, and on the load force F. In general, these rates can be parameterized in the factorized form

$$\omega_{ij} = \omega_{ij,0}\, \Phi_{ij}(F) \quad \text{with} \quad \Phi_{ij}(0) \equiv 1, \tag{3.1}$$

[2] For backward steps, the transition between the states (ED) and (DE) may also play a role [44], a picture supported by recent experiments on mutant kinesins that are more prone to backward stepping [20]. The two different mechanical transitions were also studied in Ref. [63].

where the dependence on the nucleotide concentrations is embedded in the zero force rate $\omega_{ij,0}$ and the force dependence is described by the factor $\Phi_{ij}(F)$ [49, 61]. These factors are subject to constraints to fulfill detailed balance: For all chemical transitions, the force factors $\Phi_{ij}(F)$ satisfy $\Phi_{ij}(F) = \Phi_{ji}(F)$; for the mechanical stepping transitions between states (DT) and (TD) [states 2 and 5 in Fig. 3.1b], $\Phi_{25}(F) = \Phi_{52}(F) \times \exp(-F\ell/k_BT)$ with the step size ℓ [65].

Compared to a mechanical forward step, which is completed within μs, the chemical transitions are rather slow and take several ms. Thus, the chemical reaction paths are explicitly accessible to experiments and experimentally obtained reaction rates can be implemented as the transition rates of the network model [61]. One important property of these networks is that they involve several motor cycles, which provide the free energy transduction between ATP hydrolysis and mechanical work. As one varies the nucleotide concentrations and the external load force, the fluxes on these cycles change and different cycle fluxes dominate for different parameter regimes. In this sense, the chemomechanical networks of a single motor as introduced in [61] contain several competing motor cycles. Imposing cyclic balance conditions [62] on all motor cycles ensures that the network description satisfies both the first and second law of thermodynamics.

3.3.1.2 Motor Pair Network

To extend the network description to coupled motors, we consider a pair of two kinesin-1 dimers that are attached to the same cargo and walk on the same filament. We refer to the two motors in the pair as the leading and the trailing motor, respectively, according to their relative positions in the direction of motion.

The modeling so far points to two key questions: What happens if one of the motors dissociates from the filament? And second, how does the translocation of one of the motors influence the motor pair system? For single motors, the answers are rather simple because the single motor run is terminated when the motor dissociates from the filament and the unbound motor is not spatially restricted. For the motor pair, unbinding from and rebinding to the filament provides an alternating sequence of 1-motor runs, where the cargo is pulled by one active motor, and 2-motor runs, where the cargo is actively pulled by both motors, as outlined in the upper row of Fig. 3.2. During 1-motor runs, the dynamics of the bound or active motor can be described by a random walk on the single motor network as discussed above. The only difference to the case of a single motor is that the average dwell time in any state i now also involves the rebinding rate of the second (unbound or inactive) motor. A 1-motor run is terminated either by unbinding of the remaining motor, which corresponds to the termination of the motor pair walk, or by rebinding of the inactive motor, which initiates a 2-motor run. During 2-motor runs, the state-space consists of combinations of the 7 chemical states of the individual motors, i.e., $7^2 = 49$ states.

Concerning the coupling of the motor pair, we consider the flexible stalks of the kinesin motors as linear springs. Since both springs are only coupled via the cargo, which is taken to be rigid, we can effectively describe the system by one linear spring

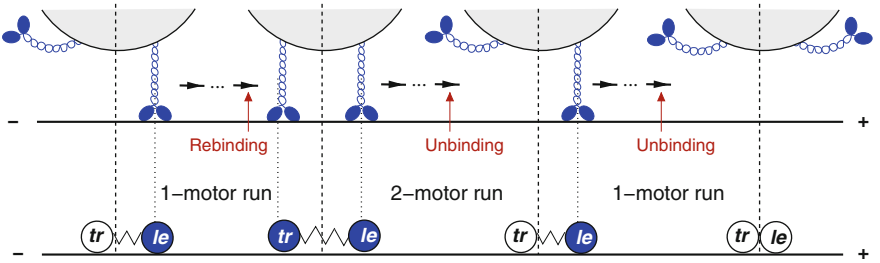

Fig. 3.2 Motor pair walk for two kinesin motors (*blue*), each of which has two motor heads. Both motors are attached to the same cargo (*light gray*) and walk along the same filament (*black line*). A reduced representation describes such a system in terms of 2-motor 'particles' connected by an effective spring. As long as both motors are attached to the filament and, thus, active as indicated by the blue 'balls' they perform a 2-motor run. After unbinding from the filament, an active motor becomes inactive as indicated by the white 'balls'. If the cargo is pulled by only one active motor, the cargo performs a 1-motor run until it either unbinds as well, leading to an unbound motor pair, or until the inactive motor rebinds to the filament and the cargo starts another 2-motor run

as indicated in the bottom row of Fig. 3.2. As a result, we obtain a one-dimensional description of the motor pair, consisting now of two motor particles which are connected via one linear spring with an effective spring constant, the coupling parameter K, and the (dimensionless) spring extension ΔL, which corresponds to the extension of the motor–motor separation (in multiples of the step size). This coupling generates the elastic force

$$F_{\mathrm{tr,le}} = -\Delta L \ell K = -F_{\mathrm{le,tr}} \tag{3.2}$$

$F_{\mathrm{tr,le}}$ between the two motors, as soon as one of these motors is spatially translocated, i.e., when it performs a mechanical step with the kinesin stepsize ℓ. We consider this interaction force as an external load on the individual motor, which thus enters the transition rates, in the form

$$\begin{aligned} \omega_{ij,le} &= \omega_{ij,0}\, \Phi_{ij}(F_{\mathrm{le}}) \\ \omega_{ij,tr} &= \omega_{ij,0}\, \Phi_{ij}(F_{\mathrm{tr}}), \end{aligned} \tag{3.3}$$

compare Eq. (3.1). In these latter relations, we used the convention that resisting forces are positive, whereas assisting forces are negative. Therefore, the forces that enter these relations are $F = F_{\mathrm{le}}$ with $F_{\mathrm{le}} \equiv -F_{\mathrm{tr,le}}$ for the leading motor and $F_{\mathrm{tr}} \equiv -F_{\mathrm{le,tr}}$ for the trailing motor. Concerning the influence of coupling on the transition rates of the motor pair system, inspection of Eq. (3.3) shows that the force arising from a mechanical step of one motor during a 2-motor run affects *all* chemical and mechanical transition rates of *both* motors.

Three variables span the state-space of the motor pair, the individual motor states $i = i_{\mathrm{le}}$ and $i = i_{\mathrm{tr}}$ of the leading and the trailing motor, and the spring extension ΔL (which we define here as a dimensionless quantity, in multiples of the step size ℓ), as shown in Fig. 3.1c. In general, the motor pair states form a stack of layers, each of which corresponds to a fixed value of ΔL. For simplicity, only the single layer with

$\Delta L = 0$ is shown in Fig. 3.1c. All chemical transitions take place within this layer, but mechanical steps during 2-motor runs are transitions to a neighboring ΔL-layer. Note that a forward step by the leading motor and a backward step by the trailing motor have the same effect on the spring extension. Rebinding and unbinding events take place between the single motor states $i = 7$ and $i = 0$ within this layer, whereas an unbinding event emanating from any other ΔL-layer always leads to the $\Delta L = 0$-layer. As a result, we obtain a uniquely defined chemomechanical network for the motor pair. Although this network is rather complex and contains a large number of states, transitions, and motor cycles, it involves only two parameters in addition to the single motor parameters: the coupling parameter K as well as the rebinding rate π of a single motor.

In experimental studies, the values of these two parameters are typically not known, but can be deduced from the statistical properties of the trajectories [49]. This deduction is facilitated by the following separation of parameters: The properties of a 1-motor run depend on the rebinding rate, but not on the coupling parameter, whereas 2-motor runs depend on the coupling parameter, but not on the rebinding rate. This feature of the pair network also allows us to study the influence of these motor pair parameters separately in computational studies. Thus, on the one hand, an analysis of the statistical properties of the motor pair trajectories gives access to the motor pair parameters K and π. On the other hand, it also allows to study the properties of the motor pair properties such as its average velocity, run length, and run time, once these two parameters are known (or as functions of these parameters). Because the chemomechanical network approach explicitly incorporates the different chemical configurations of the four motor heads, it also allows the calculation of quantities such as motor pair efficiency or operation regimes that are not directly accessible within other, more coarse-grained descriptions that we discuss next.

3.3.2 Stochastic Stepper Models

To understand the dynamics of coupled motors, it has proven useful to use simplified descriptions of molecular motors as stochastic steppers. In such a description, the chemistry is effectively incorporated into a single stepping rate and the focus is on the coupling of the motors. The advantage of such a coarse-grained description is the reduced number of parameters, which can be obtained from experimental studies. This type of approach, which has been used in several studies of cooperative motors [7, 8, 17, 18, 26, 54, 93, 101] provides a powerful conceptual framework for analyzing experimental data as well as to address generic aspects of cooperative molecular motors.

3.3.2.1 A Single Molecular Motor as a Stochastic Stepper

The dynamics of a single molecular motor consists of three basic processes, stepping along a filament as well as unbinding from and binding to this filament. To account for

the stochastic nature of these processes, each process is described by a transition rate.[3] In this way, the complex chemomechanical process of stepping is simplified into a single transition. However, the rate of that transition may be dependent on external control parameters that influence the chemomechanical cycle, such as an external load force or nucleotide concentrations. For example, the (forward) stepping rate α is typically force-dependent and can be related to the experimental force–velocity relation $v_{\mathrm{si}}(F)$ of a single motor via

$$\alpha \equiv \frac{v_{\mathrm{si}}(F)}{\ell} \tag{3.4}$$

with the step size ℓ of the motor. Likewise, unbinding from the filament is described by the force-dependent rate

$$\varepsilon_{\mathrm{si}}(F) \equiv \frac{1}{\langle t_{\mathrm{si}}(F)\rangle} \tag{3.5}$$

that can be determined from the measured average binding or attachment time $\langle t_{\mathrm{si}}\rangle$.[4] The third process, binding, is a rather complicated process, which depends on the precise geometry and other factors. Since very limited experimental data is available, it is often described by a force-independent rate π, based on the argument that typically elastic strain in the unbound motor is expected to relax upon unbinding. However, force-dependent binding rates have also been used, e.g., in Refs. [26, 66], see also the discussion in Ref. [8].

The general description introduced so far depends on the force velocity relation $v_{\mathrm{si}}(F)$, the step size ℓ, the unbinding rate $\varepsilon(F)$, and the binding rate π of a single motor. All these quantities can be measured and depend on the type of motor under consideration. Most of them have been measured for various motor species. Typical parameter values are summarized in Table 3.1. In the following, we use specific values as experimentally determined for kinesin-1 motors.

The force–velocity relation has been measured in optical trapping experiments. Typically, the velocity of the motor decreases with increasing load force F until it vanishes under the so-called stall force F_{s} [19, 21, 32]. Here, we use the following sign convention of the force: load forces opposing the stepping direction of the motor are taken to be positive, whereas negative forces are assisting forces pulling in the direction of the motor's stepping. A good approximation for the force velocity relation of kinesin-1 is the piecewise linear function

[3] Thus, we implicitly assume an exponential dwell time distribution.

[4] The index 'si' is used to indicate explicitly the unbinding rate and average binding time of a single motor. The corresponding quantities for a single bound motor in a complex of several motors (e.g., in a motor pair as discussed below) are denoted by ϵ_1 and t_1 respectively. These quantities are closely related to the single motor parameters, but there are some subtleties: While $\epsilon_1 = \epsilon_{\mathrm{si}}$, the dwell time in the 1-motor bound state (or the average duration of a 1-motor run) for cooperative motors also depends on the binding rate π of the second motor or any other in a system with more than 2 motors, $t_1 = (\epsilon_1 + \pi)^{-1} < t_{\mathrm{si}}$.

Table 3.1 Overview of parameters for the different molecular motors kinesin-1, dynein, myosin V, and myosin VI

Parameter	kinesin-1	dynein	myosin V	myosin VI
Binding rate π [s^{-1}]	4.7* [57], 5* [5, 57]	1.6* [72]	–	–
Step size ℓ [nm]	8 [91]	8 [32]	36 [21]	36 [74]
Stall force F_s [pN]	6 [82, 85], 5 [23], 7 [19]	7 [87] 1.1 [67]	1.7 [21], 3 [70]	2.8 [78]
(Force-free) velocity v [nm/s]	1,000 [82], 490 [79]	650* [72], 700 [50]	400 [21], 380 [1]	150 [1], 291 [78]
(Force-free) unbinding rate ϵ_0 [s^{-1}]	1 [82], 0.6 [79]	0.27* [72], 0.16 [68]	0.48 [70], 0.3 [1]	0.25 [1], 1.3 [78]
Detachment force F_d [pN]	3 [82]	1.1* [72]	4* [1]	2.6* [1]

The values marked by an asterisk are inferred indirectly by theoretical modeling of experimental data

$$v_{si}(F) \equiv \begin{cases} v & F < 0 \\ v(1 - F/F_s) & 0 \le F < F_s \\ 0 & F \ge F_s, \end{cases} \tag{3.6}$$

see Fig. 3.3b, but more complicated functional forms and parameterizations can also be used [7]. The force-dependence of the unbinding rate is described by the exponential form

$$\varepsilon_{si}(F) \equiv \varepsilon_0 \exp(|F|/F_d). \tag{3.7}$$

Note that by using the absolute value of the force, we do not distinguish between different pulling directions. This type of dependence is suggested on theoretical grounds according to Kramers' rate theory [53] and Bell's equation [6] and supported by measurements of the force-dependence of the run length [82]. The force-dependence of the unbinding rate is currently revisited by several labs for different types of motors. Deviations from this exponential increase have recently been reported for dynein motors, with an exponential increase for small forces but catch-bond-like behavior, i.e., a decrease in the unbinding rate, for forces around the stall force [55, 59].

Since it is difficult to measure the binding rate π directly, its value has been determined by fitting theoretical models to experimental data. In this way, a binding rate $\pi \simeq 4.7\,s^{-1}$ is obtained from an experiment where kinesin-1 motors extract membrane nanotubes from vesicles [57]. A similar value has been reported in a study fitting the run length distribution of beads transported by several kinesin-1 motors [5]. For other types of motors, most of the parameters have also been determined experimentally; the corresponding parameter values are summarized in Table 3.1.

The simple stochastic stepper description of a single motor incorporates those properties of single motors that are relevant for large-scale cargo transport. Furthermore, the theoretical framework described here can easily be extended, for example,

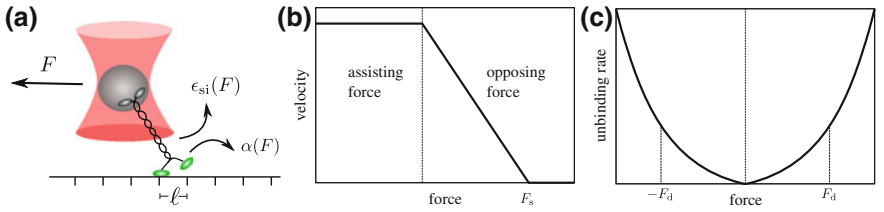

Fig. 3.3 Force-dependent dynamics of a single motor: **a** Schematic setup of a typical single molecule experiment, in which a single kinesin is held with an optical trap that exerts the force F on the motor in the direction opposite to its walking direction. The motor steps forward with the force-dependent stepping rate $\alpha(F)$ and the step size ℓ. Force-dependent unbinding of the motor from the filament is described by the rate $\varepsilon_1(F)$. **b** Piecewise-linear parametrization of the force velocity relation $v_{si}(F)$, from which the stepping rate is determined via $\alpha(F) = v_{si}(F)/\ell$. **c** Parameterization of the force-dependent unbinding rate of the single motor. The stall force F_s in (**b**) and the detachment force F_d in (**c**) provide the basic force scales for the single motor behavior

to include backward steps or functional dependencies on other parameters such as the nucleotide concentrations [7]. Incorporating additional features of single motors usually requires additional parameters that need to be determined either directly from experiments or calculated from more microscopic models such as the chemomechanical networks described above. In the case of backward stepping, the forward stepping rate and the backward stepping rate can be determined from the force–velocity relation and the force-dependent ratio of forward to backward steps [8, 61]. The latter quantity has been measured for kinesin-1 [19].

3.3.2.2 Two Elastically Coupled Molecular Motors

In the following, we use the coarse-grained single motor description that we introduced above to study two elastically coupled molecular motors. As a generic case, we focus on two identical motors coupled via their stalks to a common cargo. Below, we use this model to determine the time t_2 that two motors stay simultaneously attached to the filament and the resulting velocity v_2 of the cargo, two key quantities for an even more coarse-grained description of transport by a motor pair as described at the end of this section. In general, these two quantities are expected to depend on the single motor dynamics and on the coupling. Because of the stochastic stepping of the motors, the elastic elements between them are stretched (or compressed) and relaxed. Thus strain forces are generated that in turn influence the stepping of the motors [7].

Assuming a linear force-extension relation of the elastic coupling, the only parameter, in addition to the single motor parameters, is again the coupling strength K. Since the motors step in a discrete manner, the induced strain forces have discrete values

$$F_i = i\ell K, \tag{3.8}$$

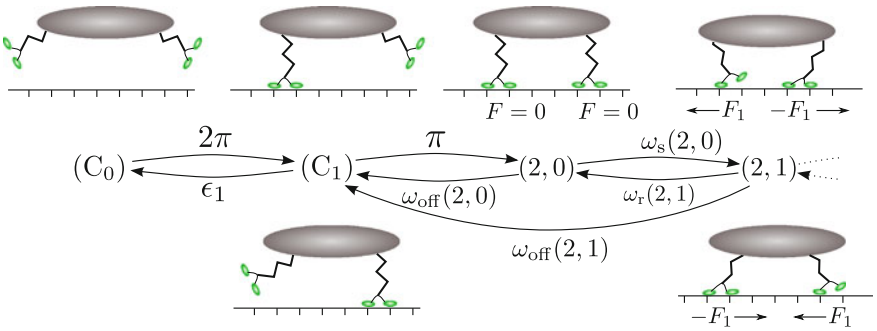

Fig. 3.4 State-space of a cargo transported by two identical motors. In state (C_1) the cargo is transported by only one motor. The other states $(2, i)$ correspond to different strain forces between two motors simultaneously pulling the cargo. In state $(2, 0)$, the motors are bound with relaxed linkers such that there is no force between them. When one of the motors performs a step, a strain force is generated between the two motors (the same strain is generated by stepping of either motor, therefore there are two configurations corresponding to the same state). Thus, stepping transitions between the states lead to the stretching or compression or to the relaxation of the elastic linkers. Unbinding of a motor occurs with rate ω_{off}

where ℓ is the motor step size, K the coupling strength and i the distance (number of steps) between the motors.

The state of the two motors is now described by a discrete state-space, in which every state is characterized by the number of motors bound to the filament and, when both are bound, the discrete extension of the elastic linker between the motors (or the associated force), see Fig. 3.4. The states with no or one motor bound to the filament are denoted by (C_0) and (C_1), respectively. The states with two motors bound are denoted by $(2, i)$, where i is the discrete distance between the motors.[5] Thus, in state $(2, 0)$, the linkers between the motors are relaxed. When one of the motors steps, the strain force $F_1 = \ell K$ is built up between them in such a way that one motor is pulled backwards with force F_1 and the other motor is pulled forwards with force $-F_1$, see state $(2, 1)$ in Fig. 3.4. Because we do not distinguish between the two motors, there are two configurations for this state.

Transitions between the different states $(2, 1)$ are associated with stepping of the motors. We denote the corresponding transition rates by $\omega_{\text{s}}(2, i)$ and $\omega_{\text{r}}(2, i)$, depending on whether the transition stretches (or compresses) or relaxes the linkers. These transition rates depend on the state of the motor pair and are related to the single motor stepping rates via

$$\omega_{\text{s}}(2, i) = \alpha(F_i) = v_{\text{si}}(F_i)/\ell \tag{3.9}$$

[5] It is convenient to introduce a highest state $(2, N)$ to reduce the network to a finite number of states. The state $(2, N)$ corresponds to a very large extension between the motor. Such a configuration is unlikely, because the motors typically unbind before reaching this state. Nevertheless, one has to check that the results do not depend on the choice of the value of N.

and

$$\omega_{\mathrm{r}}(2,i) = \alpha(-F_i) = v_{\mathrm{si}}(-F_i)/\ell. \tag{3.10}$$

for all states $(2,i)$ with $i > 0$ and

$$\omega_{\mathrm{s}}(2,0) = 2\alpha(0) = 2v_{\mathrm{si}}(0)/\ell \tag{3.11}$$

for state $(2,0)$. In these expressions, $v_{\mathrm{si}}(F)$ denotes the force-velocity relation of a single motor.

Transitions between the states (C_0) and (C_1) correspond to binding and unbinding of a motor, with rates given by the single-motor parameters. Unbinding of the bound motor in state (C_1) occurs with the single-motor unbinding rate ϵ and leads to state (C_0). The reverse transition is given by binding of one motor. Because either of the motors may bind, the rate for this transition is 2π. Likewise, binding of the second motor occurs with rate π. We take this transition to lead to state $(2,0)$, i.e., we assume that the second motor binds in such a way that upon binding there is initially no strain between the motors. Finally, unbinding of one of the two bound motors, i.e., a transition to state (C_1) may occur from any state $(2,i)$ and its rate is force-dependent,

$$\omega_{\mathrm{off}}(2,i) = 2\varepsilon_1(F_i). \tag{3.12}$$

3.3.2.3 Effective Parameters of Transport by Two Bound Motors

While the dynamics of the motor pair can be studied using the model as described in the previous section, additional insight into the cargo transport can be obtained by lumping the states $(2,i)$ into one state (C_2) with two motors bound to the filament and to determine an effective stepping rate or an average velocity v_2 for this state as well as an effective unbinding rate ϵ_2 for one of the two motors, i.e., a transition rate to state (C_1). The resulting coarse-grained description was originally proposed in Ref. [51], well before the more microscopic description. Coarse-graining of the microscopic model, however, now allows to obtain the parameters of state (C_2) in a systematic way.

To determine the properties of the state (C_2), we can focus on its substates $(2,i)$ and treat state (C_1) as an absorbing state. Thus, all transitions associated to unbinding of a motor become transitions into the absorbing state with transition rates $\omega_{\mathrm{off}}(2,i)$. We then consider a Markov process on this network with the initial condition that all trajectories start immediately after binding of the second motor, i.e., in state $(2,0)$. The binding time or average dwell time in the two-motors-bound states is then obtained as the mean first passage time to absorption, the effective unbinding rate as the inverse of the binding time, and the velocity as the average stepping rate before absorption. We note that unbinding of motors is a mechanism for relaxing strain between the motors, because the unbinding rate increases with increasing force and rebinding occurs under zero load. Thus, simply neglecting unbinding, as done in some studies [93], will overestimate the probability of states $(2,i)$ with large i, i.e.,

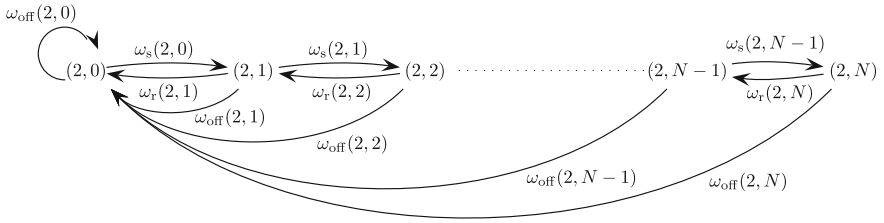

Fig. 3.5 Closed network for calculating the probability distribution before unbinding of one motor: Starting from the network shown in Fig. 3.4, only the states $(2, i)$ in which both motors are simultaneously bound to the filament are considered and the state (C_1) is treated as an absorbing state. The network is closed by redirecting all transitions that lead into the absorbing state back into the initial starting state $(2, 0)$

with large strain forces and therefore overestimate the effect of those forces. Indeed, neglecting unbinding typically leads to a strongly reduced velocity for two coupled kinesin-1 motors [47, 93], in contrast to what is found in the model with unbinding [7] and to what is observed experimentally [79].

An intuitive way to calculate the quantities characterizing state (C_2) is based on a method proposed by Hill [38, 39]. The basic idea is to use the ensemble average instead of the time average, which makes it unnecessary to solve the time-dependent problem. To construct a network, whose steady state probability distribution is the steady state probability distribution before absorption of the original network, all transitions into the absorbing state are redirected to the initial state. Intuitively, this procedure can be understood as concatenating many trajectories, in the same way as one would do it in a computer simulation, namely by starting the next trajectory immediately after the one before has reached the absorbing state. Such a closed network is shown in Fig. 3.5. The probability distribution $P_{2,i}$ for the closed network is determined by solving the steady state of the master equation

$$\begin{aligned}
\partial_t P_{2,0} &= -[\omega_{\rm s}(2,0) + \omega_{\rm off}(2,0)]P_{2,0} + \omega_{\rm r}(2,1)P_{2,1} + \sum_{j=0}^{N} \omega_{\rm off}(2,j)P_{2,j} \\
\partial_t P_{2,i} &= \omega_{\rm s}(2,i-1)P_{2,i-1} - [\omega_{\rm s}(2,i) + \omega_{\rm r}(2,i) + \omega_{\rm off}(2,i)]P_{2,i} \\
&\quad + \omega_{\rm r}(2,i+1)P_{2,i+1} \\
\partial_t P_{2,N} &= \omega_{\rm s}(2,N-1)P_{2,N-1} - [\omega_{\rm r}(2,N) + \omega_{\rm off}(2,N)]P_{2,N},
\end{aligned} \tag{3.13}$$

where the middle equation is valid for $0 < i < N$. Here $P_{2,i}$ is the probability of being in state $(2, i)$ before absorption. Together with the normalization condition, the steady state of this set of equations can be solved with a backward substitution, since $P_{2,N}$ only depends on $P_{2,N-1}$. Now, the inverse mean first passage time or the effective unbinding rate (the rate of being absorbed), ϵ_2, is given by the probability current into the absorbing state, i.e.,

$$\epsilon_2 = \frac{1}{t_2} = \sum_{i=0}^{N} \omega_{\text{off}}(2, i) P_{2,i}. \tag{3.14}$$

Averaging the stepping rates of both motors, weighted with the probabilities $P_{2,i}$, we obtain the velocity as

$$v_2 = \frac{\ell}{2} \sum_{i=0}^{N} [\alpha(F_i) + \alpha(-F_i)] P_{2,i}. \tag{3.15}$$

Once these two parameters have been obtained, the transport properties for a cargo pulled by two motors can be obtained using the theoretical framework of Ref. [51], which is discussed below. Specifically, the average velocity of the cargo, i.e., averaged over the states (C_1) and (C_2), is obtained as

$$v_{\text{ca}} = \frac{\pi v_2 + \epsilon_2 v_1}{\pi + \epsilon_2}, \tag{3.16}$$

where v_1 is the velocity when only one motor is bound. In the absence of an external force, $v_1 = v$, whereas in the presence of an external force, it s given by the force-velocity relation (3.6). Likewise, the average run length of the cargo, the distance moved before complete unbinding, is obtained as

$$\langle \Delta x_{\text{ca}} \rangle = \frac{\pi v_2 + \epsilon_2 v_1}{\epsilon_1 \epsilon_2}. \tag{3.17}$$

The advantage of using this combination of the explicit description of substates $(2, i)$ and the coarse grained description with states (C_0), (C_1) and (C_2) is that different parameterizations for the single motors or different couplings can be implemented rather easily and their cooperative behavior can be deduced in a computationally inexpensive manner [7].

3.3.2.4 Motility States of a Cargo and Semistochastic Approaches

Many experimental studies report trajectories (or kymographs) of labeled cargoes. Unless experimental methods with very high spatial and temporal resolution are used, e.g., [58, 98], discrete steps are not resolved and the cargo is seen to perform continuous motion with a velocity v, suggesting a deterministic description of the cargo movement of the cargo. Such a description [51] can be considered as resulting from the coarse-graining of a more microscopic description that replaces stochastic stepping by constant cargo velocities that characterize the different states of the cargo, for example, the states (C_1) and (C_2) discussed above.

The value of the cargo velocity is determined by the dynamics of the motors. If the cargo imposes a substantial load for the motors, for example in a viscous

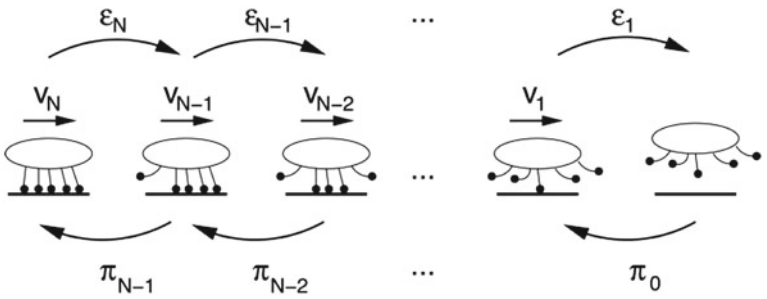

Fig. 3.6 A cargo particle is transported by N motors. Each state is characterized by the number of bound motors. In each state the cargo has velocity v_n, a motor unbinds from the filament with rate ε_n and an additional motor binds to the filament with rate π_n (reprinted from Ref. [51])

medium, a larger number of motors actively pulling on the cargo can result in higher speed [31, 51]. Since motors unbind and rebind to the filament, the velocity of such a cargo changes when the number of bound motors change. Therefore, a rather general coarse-grained description for cooperative cargo transport by molecular motors can be obtained by a discrete state-space with cargo states associated with the number of bound motors [51]. Transitions between these states correspond to binding and unbinding of motors, see Fig. 3.6. Thus, the model is semistochastic, describing the cargo movement (based on rapid steps) as a deterministic process and motor binding/unbinding, which happens on longer timescales, as stochastic processes. In principle, the parameters of this model, the velocities and unbinding rates can be obtained by systematic coarse-graining as described above. However, this has so far not been done for more than two motors. For cases with more than two motors, the rates have been obtained by making plausible assumptions such as weak coupling between the motors and equal sharing of load forces [51, 72]. This approach allows us to calculate dynamical properties of the cargo, like the run length and run time of a cargo transported by teams of motors. Such studies have been done for unidirectional transport by a single team of motors [51], for bidirectional transport by two teams of motors [72], for transport by motors with different velocities [56], and for combined directed and diffusive transport by active and inactive motors [10, 75].

If a cargo is transported by two teams of antagonistic motors, i.e., by motors that walk in opposite directions, the cargo is transported in a bidirectional manner, changing direction every few seconds. A theoretical description for this transport mode also starts by identifying discrete states associated with the numbers of bound motors of both types, see Fig. 3.7. Transitions between the states arise from binding and unbinding of the motors. Since the unbinding rate depends on the external force, motors can pull each other from the filament resulting in a tug-of-war. Such a tug-of-war displays a rich pattern of motility depending on the single motor parameters [71–73]. In particular, the analysis of this model showed that mechanical interactions of the motors mediated by the two teams pulling on each other is sufficient to generate rapid bidirectional movements [72]. No specialized coordination complex,

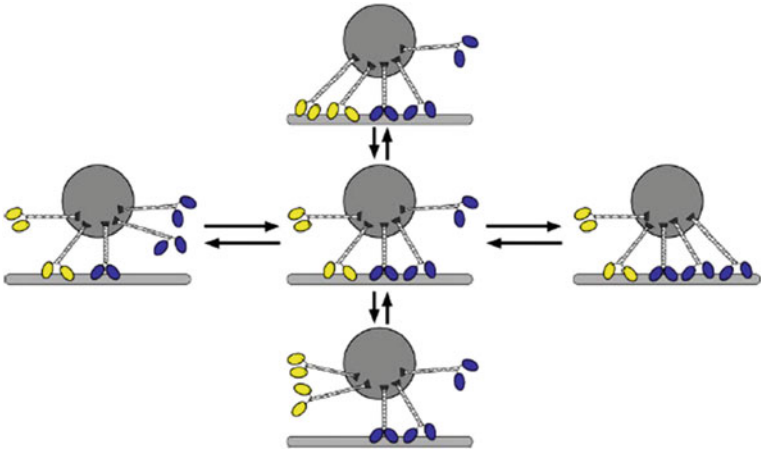

Fig. 3.7 A cargo with 3 plus (*blue*) motors and 2 minus (*yellow*) motors is pulled by a fluctuating number of motors bound to the filament. The different states are defined by the number of bound motors. Only five of 12 possible states are displayed (reprinted from Ref. [72])

as proposed earlier (see, e.g., Ref. [95]), is required. Later experiments provided direct evidence for such mechanical interaction between motors [36, 84], which can be seen as an unavoidable physical constraint on the coordination of motors with opposite directionality. Some recent experimental studies also indicate that not all observations can be interpreted by mechanical interactions alone [55, 59], suggesting an additional layer of biochemical regulatory mechanisms regulating the tug-of-war, as emphasized in the theoretical studies [73].

The approach described so far can be extended to account for diffusive movements of the cargo along the filaments as observed experimentally [2]. For cargo states in which the motors diffuse, the velocity v of the cargo vanishes. To account for the diffusive dynamics (or, likewise, for biased diffusive dynamics) one can describe the position of the cargo again in a stochastic fashion using an over-damped Fokker-Planck equation [77]. In this way, the motion of the spatial coordinate of the cargo in a state (i) is described by a Fokker-Planck operator $\mathscr{L}_i$. Extending the master equation to account for the time evolution of this coordinate explicitly leads to

$$\partial_t p_i(x,t) = \sum_j \omega_{ji} p_j(x,t) - \sum_j \omega_{ij} p_i(x,t) + \mathscr{L}_i p_i(x,t). \tag{3.18}$$

Here $p_i(x,t)$ is the probability that the cargo is in state (i) at the coordinate x at time t. The transition rate from state (i) to (j) is given by ω_{ij}. Within the framework of Fokker-Planck operators one can describe a wide range of motility patterns. Two important limiting cases are purely diffusive motion, which is represented by

$$\mathscr{L} = D\partial_x^2 \tag{3.19}$$

and deterministic motion with constant velocity v, represented by

$$\mathscr{L} = -\partial_x v. \tag{3.20}$$

If one is only interested in average values of observables such as the run length and the average binding time, one can avoid to explicitly solve the Fokker-Planck equation by using again the Hill method. This approach has been used in Ref. [10] to study how the presence of inactive, but diffusing motors enhances the processivity of actively pulling motors.

3.3.3 Explicit Descriptions of the Geometry of Motor–Cargo Complexes

Finally, studying some aspects of molecular motor complexes requires geometric information about the system. A rather obvious example is effects of the arrangement of the motors on the cargo or in a multi-motor complex: Does it make a difference whether motors are attached to a cargo in one specific location or randomly distributed on a large cargo? What impact does the distance between two motors in a motor pair have? Does steric hindrance between motors play a role? These aspects have been studied in less detail than the stochastic network models discussed so far. Moreover, the construction of models that incorporate three-dimensional spatial information is less systematic than for the stochastic networks. In this section, we give a brief review of what has been done, without going into the technical details. We then discuss one such approach [52] in more detail to highlight some issues that arise in a geometric description of systems of cooperative motors.

In models that describe the spatial structure of the motor–cargo complex, motors are typically represented by a few degrees of freedom, namely their point of attachment to the filament (the 'head'), their point of attachment to the cargo and an elastic element between these two points, which may be a linear spring, a cable-like spring, or an empirically defined nonlinear spring. The position of the attachment point to the cargo is determined by the position and orientation of the cargo. Once the head is attached to the filament it moves like a stochastic stepper, but the force it experiences is now calculated according to a three-dimensional force balance. The movements of unbound heads are typically not described explicitly. Rather, unbound heads may bind to the filament according to a rate that depends on the relative location of the attachment point and the nearest sites on the filament, accounting for the distance to the filament and possibly for steric hindrance by the cargo or by other motors.

Approaches of this type have been used to address a number of issues. One study, in which our group was involved [52], has addressed the sharing of a viscous force among motors that are randomly distributed on a cargo and compared different elastic elements (linear and cable-like springs with different lengths). A similar study by Erickson et al. [28] investigated the impact of the geometric arrangement of motors

by comparing motors randomly distributed on a cargo and clustered motors and found that cooperation is more efficient in the clustered case, with larger run lengths. Finally, Driver et al. [26] used geometric force balance to determine transition rates in a Master equation approach used for a systematic comparison with optical trapping experiments on a two-kinesin-1 complex. The models used in these studies differ in various aspects, such as the description of the cargo (as simply the center of mass of the motors or as a diffusing particle), the choice of elastic element between the motor head and the cargo, and the inclusion of hydrodynamic effects and of steric hindrance. These differences make the comparison of the models quite difficult, and the relative importance of the various ingredients of these models remains to be elucidated.

We now describe the approach by Korn et al. [52] in some more detail in order to point out a few issues that arise in a description of the motor complex geometry. In that model, the motion of a spherical cargo particle is described using a Langevin equation with 6 degrees of freedom (its position in a three-dimensional space and its orientation) and with a position-dependent mobility matrix that accounts for hydrodynamic effects due to the presence of a wall (the coverslide on which the filament is immobilized). The motors are randomly distributed on the cargo and, when bound to the filament, move by stochastic stepping as described in Sect. 3.3.2 above. The motor "tail", the link between the motor head on the filament and the attachment point on the cargo, is described as an elastic element (either a linear spring or a cable-like spring). Thus, the cargo particle is subject to the forces mediated by the motor springs, viscous forces from the surrounding fluid and random forces that lead to the diffusion of the cargo particle around the equilibrium position given by the balance of the motor forces. External forces acting on the cargo can also be incorporated. In particular, because hydrodynamic effects are already incorporated in the mobility matrix, this approach is particularly suited to study hydrodynamic forces, arising, e.g., from shear flow.

Within this description of the motors, the elastic forces act along the direction of the springs, i.e., under an angle to the direction of motion. It is thus not entirely clear how this force should affect the stepping rates, as in the experiments the forces are typically exerted in the direction parallel to the filament. Therefore, an additional assumption has to be made at this point and simulations to validate this modeling assumption are required. In Ref. [52], the spring force was projected onto the direction of motion and the projected force was used in a linear force dependence of the stepping rate. This assumption led to a linear force-velocity relation in simulations mimicking an optical tweezers experiment with an external force applied to the cargo in the direction antiparallel to the direction of motion. Obviously, more complex force dependencies can be implemented, but in any case, the assumed force dependence needs to be validated by comparison to experimental data or to a desired simplified force-velocity relation.

A second issue that deserves a few comments is how binding of a motor to the filament is treated. In the approach of Korn et al. [52], the position of unbound motor heads is not described explicitly. Unbound motor heads perform rapid tethered diffusion with the ends of their tails fixed by the position of the cargo. Their rebinding

to the filament is therefore determined probabilistically with a rate that depends on two factors, a bare binding rate for a motor close to the filament and a probability that the motor is indeed close to the filament, i.e., within some capture distance to a free binding site on the filament. The latter distance can be determined by considering the overlap between the binding sites and the shell on which the tethered motor head diffuses.

3.3.4 General Modeling Strategy and Integration of Models on Different Scales

We conclude our discussion of theoretical methods with some general remarks about the choice of a theoretical description and the construction of suitable models. The theoretical approaches described above provide different description of cooperative transport by several motors or of motor complexes, but they follow the same general modeling strategy.

The first step is to choose a level of theoretical description that is appropriate to study the questions of interest. This choice involves both the desired output of the model and the prior knowledge available as its input. The desired output determines how detailed the description needs to be and defines the time and length scales to be studied (if simulation time is a limiting issue, the latter may be a strong constraint). The available input, on the other hand, is critical for the feasibility by determining the number of unknown parameters. For the discrete stochastic models described above, the choice of a theoretical description ultimately leads to the identification of a set of states of the system described by a set of variables characterising these states. These variables are typically a combination of variables characterizing each individual motor (e.g., the chemomechanical states of the two motors) and variables characterizing their coupling (e.g., the force between the motors). While a motor or motor complex is in one such state, these parameters are taken to remain constant, so molecular movements on scales smaller than the chosen description are neglected.

In addition to the states, one needs to identify the transitions between the states (which are related to chemomechanical transitions of the configuration of a motor, stepping of a motor or binding/unbinding of a motor). For a multi-motor complex, these transitions are derived from the corresponding transitions of the single motors. Once the network of states linked by the allowed transition between them is set up, the transitions have to be associated with the corresponding transition rates. This is ideally done based on experimental data, but in many cases this step needs additional theoretical input. For cooperative motors, these transition rates can often be derived from the transition rates of individual motors under force, by incorporating forces arising from the coupling of the motors into the force experienced by that motor. Alternatively, one can calculate these rates from a more detailed model. An example is given by our calculation of ϵ_2 in the stepper model in Sect. 3.3.2 that can be used in the semi-stochastic theoretical description of cargo movements. Yet another option

would be to use force-dependent single-motor transition rates, but determine the force from a detailed microscopic force balance. Thus, this step, the calculation of transition rates, provides an opportunity for true multiscale approaches.

Once the rates are known, the dynamics of the system can be solved either analytically or by simulations and observables can be determined and compared with experimental data. If necessary, the model is then adjusted. The latter comparison provides a consistency check in cases where the input of the model, the transition rates, is taken directly from experimental data, and a validation step for descriptions based on assumptions about the microscopic processes and interactions. Finally, quantitative predictions can be made with such a consistent theoretical description.

3.4 Results

The methods described above have been used extensively to study cooperative transport by molecular motors. Here we highlight some results where bridging the length and timescales has been crucial. Specifically, we discuss two issues: the effect of the coupling strength on motor cooperation and the different transport regimes that can emerge when different motor types are coupled.

3.4.1 Impact of Elastic Coupling

3.4.1.1 Varying Elastic Coupling in Chemomechanical Networks

Both the chemomechanical network and the stochastic stepper model as described above are based on a complete description of a single motor. In addition to the parameters characterizing the single motor, these models have only two parameters, the binding rate π and the coupling parameter K.[6] Figure 3.8 shows some results obtained with the chemomechanical network approach for kinesin-1, systematically varying these two parameters. Figure 3.8a shows different activity regimes, regions in the parameter space, where transport is dominated by 1-motor runs and 2-motor runs, respectively. Which activity state is dominant during a motor pair walk obviously depends on the rebinding rate π, but also on the coupling parameter K, because K influences the termination rate ϵ_2 of 2-motor runs. The activity regime diagram in Fig. 3.8a shows the crossover line which separate the parameter regime in which 1-motor runs dominate the cargo run from the regime in which 2-motor runs are more likely. Along this line, both are equally probable. A small rebinding rate leads to a clear dominance of 1-motor runs for all values of the coupling parameter, whereas clear dominance of 2-motor runs is only found for relatively large rebinding rates and small coupling parameters.

[6] There may be more parameters for nonlinear couplings.

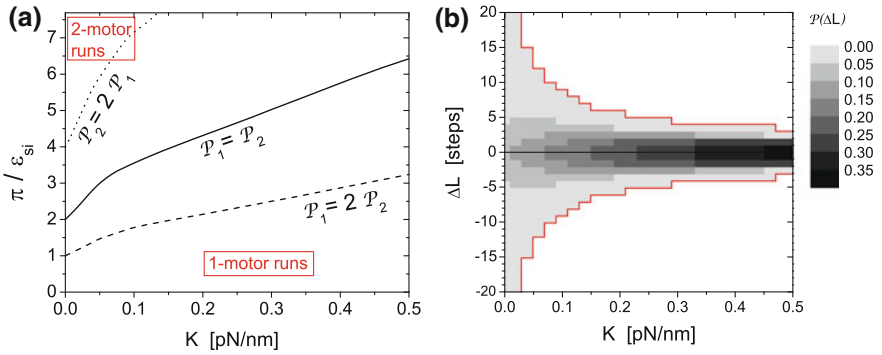

Fig. 3.8 **a** Activity regimes of a motor pair in terms of the probabilities $\mathscr{P}_1$ and / $\mathscr{P}_2$ for 1-motor and 2-motor runs: The crossover *line* $\mathscr{P}_2 = \mathscr{P}_1$ separates the parameter regime, in which 1-motor runs dominate the cargo run from the regime in which 2-motor runs are more likely. The *dashed* and the *dotted lines* are the crossover lines at which $\mathscr{P}_1 = 2\mathscr{P}_2$ and $\mathscr{P}_2 = 2\mathscr{P}_1$, respectively. **b** Contour plot of the probability distribution $\mathscr{P}(\Delta L)$ for the extension ΔL of the motor-motor separation as a function of the coupling parameter K. The *red line* indicates maximal values of ΔL observed in the simulations

From trajectories of the individual motors within a motor pair, one can deduce the distribution of the extension ΔL of the motor-motor separation as shown in Fig. 3.8b. Since we define $\Delta L \equiv 0$ for 1-motor runs, this is a property of 2-motor runs. The probability distribution $\mathscr{P}(\Delta L)$ is symmetrically distributed around the average $\langle \Delta L \rangle = 0$ for all coupling parameters, which implies that the leading and trailing motor are interchangeable. The number of accessible ΔL values decreases with increasing coupling parameter K. Within the studied range for the coupling parameter, this number varies by one order of magnitude. Measuring the width and amplitude of the distribution for the deflection ΔL one can, for instance, determine the coupling parameter K. In principle, this distribution could also be used to reconstruct the full force–extension curve for a nonlinear spring that couples the motors. We note however that the distribution $\mathscr{P}(\Delta L)$ not only reflects the interaction potential of the two motors, but also depends on their unbinding, because unbinding from a state with large ΔL with subsequent relaxation and rebinding also provides a pathway to return to small extensions ΔL.

3.4.1.2 Coupling Dependence in Stochastic Stepper Models

We briefly review the effect of varying the coupling strength in the stochastic stepper model and use this example as an illustration for how models at different scales and with different levels of detail can be integrated. Specifically, the detailed stochastic stepper model is used to determine parameters that enter the coarse-grained semi-stochastic description where all substates of the two-motor-bound state are lumped together.

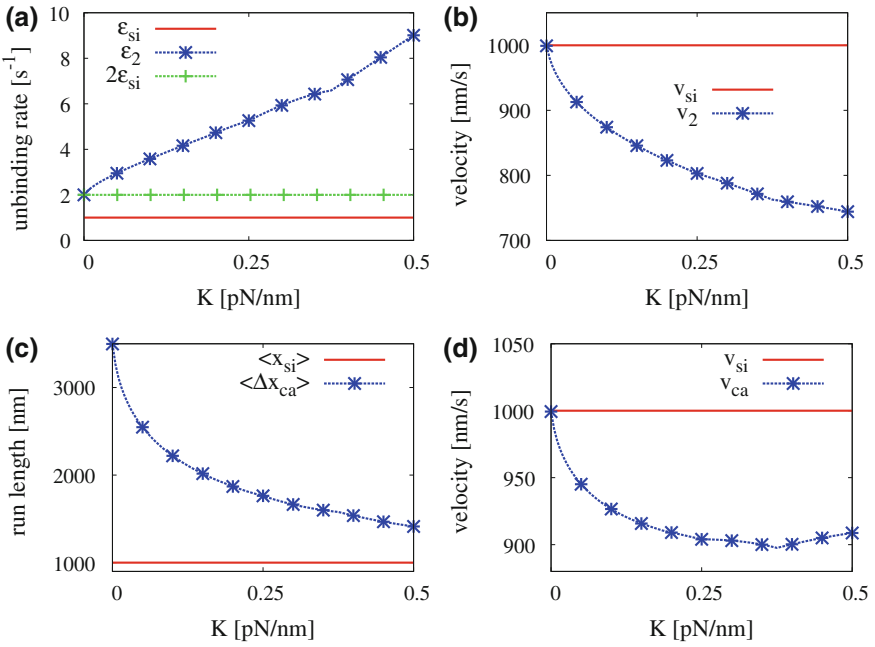

Fig. 3.9 Transport properties of an elastically coupled kinesin pair: **a** Effective unbinding rate ϵ_2, **b** average velocity v_2 of two bound motors, **c** run length and **d** average cargo velocity as functions of the coupling constant K. In all subfigures, the K-independent single motor properties are also included. The kinks in these *curves* are due to the discrete values of the force between the motors and arise when the stall force is an integer multiple of the strain force, i.e., for $K = F_s/(\ell n)$ with integer n. At these values of K, the number of states $(2, i)$ with forces *below* the stall force changes by 1

Figure 3.9a, b shows the effective unbinding rate ϵ_2 and the effective velocity v_2 as functions of the coupling strength K using parameters for kinesin-1 and assuming coupling by a linear spring. The two quantities, which are calculated via Eqs. (3.14) and (3.15), are characteristics of 2-motor runs and therefore independent of the binding rate π. The effect of coupling on the velocity is moderate with only about 15 percent reduction for strong coupling. The effect on unbinding is much more pronounced: For weak coupling, the motors unbind independently of each other, and the unbinding rate of one of them is thus twice the single-motor unbinding rate. With increasing coupling strength, the unbinding rate exhibits a strong increase, in agreement with experimental observations [79].

Using these results of the microscopic stepper model in the more coarse-grained semi-stochastic one, one can calculate the transport properties of the cargo such as the average velocity (averaged over 1-motor runs and 2-motors runs) and the cargo run length via Eqs. (3.16) and (3.17). These two quantities are plotted in Fig. 3.9c, d, also as functions of the coupling strength. Both quantities also depend on the binding rate. The dominant effect of coupling on the unbinding rate can also be seen

here: the run length decreases strongly with increasing coupling strength. The run length of the two-motor complex, however, is always larger than the run length of a single motor (which is approached for large coupling strength), i.e., the interference between the motors decreases the effect of motor cooperation, but does not reduce it below the level of a single motor. The average velocity shows even less reduction than the velocity v_2 of 2-motor runs and increases again for strong coupling, because with increasing coupling strength, 1-motor runs become more and more likely, and thus the reduced velocity of 2-motor runs contributes less and less to the average.

Nonlinear couplings have also been considered within the stochastic stepper approach [8]. For example, cable-like springs (that are linear springs with respect to stretching but exhibit no resistance to compression) leads to a much weaker effect because it takes longer to build up substantial strain forces between the two motors [8]. In addition, several studies have considered springs with a force-dependent spring constant, specifically, the case of a spring that is rather soft at low force and stiff at large forces. Such a spring can be characterized by two spring constants and is suggested by some experiments on the kinesin tail [3, 27]. The latter spring also leads to weaker coupling effects, indicating that the lower spring constant (for which building up strain requires some time) is dominant during 2-motor runs [8].

3.4.1.3 Different Types of Elastic Coupling and Cargo Geometry

Finally, the impact of the type of spring was also studied in simulations of bead movements with explicit representation of the cargo geometry. Two different types of springs were studied, a linear spring and a cable-like (or semi-harmonic) spring that behaves as a linear spring when stretched, but does not resist compression. In addition, different rest lengths were used in both cases. For all cases, run length distributions were determined from extensive simulations. The distributions were approximately given by double-exponentials, and the average run length was found to increase almost exponentially with the number of motors attached to the cargo. For the same number of motors on the cargo, the average run length was found to be longer for longer springs [52]. This result can be explained by the observation that, in this case, more motors are bound to the filament simultaneously. This means that the longer spring rest length provides more flexibility to accommodate a larger number of motors on the filament. Moreover for all rest lengths, cable-like springs lead to longer run lengths than linear springs. This has been interpreted as an effect of the average distance between the cargo and the filament, which is expected to be smaller for cable-like motors, where the springs do not induce upward forces on the cargo, than for linear-spring motors [52]. However, our more recent discussion of interference effects for nonlinear springs suggests another explanation (not mutually exclusive with the first): For cable-like linkers, forces between the motors build up more slowly than for linear springs [8], so interference effects are less pronounced. Specifically, for linear springs, forces built up because of the nonsynchronous stochastic stepping of the motors, enhance unbinding, thus effectively reducing the number of bound motors.

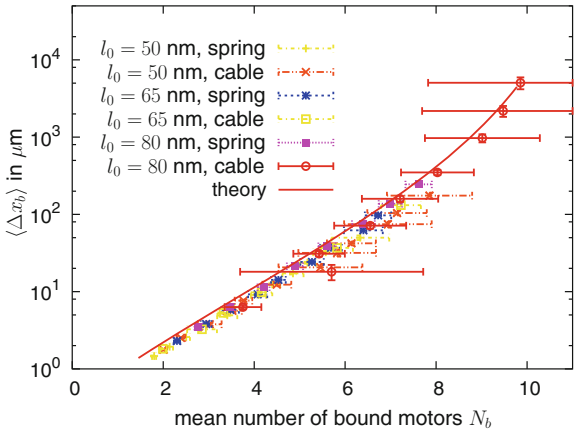

Fig. 3.10 Run length of simulated beads transported by many kinesin motors: Data for the run lengths obtained with different elastic elements collapse onto a single master *curve*, when plotted against the average number of bound motors, indicating that the number of bound motors is what effectively determines the run length (reprinted from Ref. [52] with permission from AIP Publishing)

When the average run length is plotted against the average number of bound motors, the results for all spring models collapse on a single curve (Fig. 3.10). This master curve can also be described by the theoretical expectation based on the model of Ref. [51], if the maximal number of motors able to bind simultaneously is taken from a Poisson distribution, as indicated by the solid line in Fig. 3.10. This result shows that the dependence of the run length on the geometric details is fully mediated by a modulation of motor-filament binding and that additional factors such as modulation of the stepping rate or the movement of the cargo are of lesser importance.

3.4.2 Transport Regimes

Finally, we briefly discuss some generic aspects of cooperative transport that can be understood based on the derivation of the effective parameters ϵ_2 and v_2 of 2-motor runs from the microscopic stochastic stepper model. In the absence of an external force, the stepper model is characterized by three different force scales, the stall force F_s, the detachment force F_d, and the strain force F_K that arise from coupling. The latter is defined by the force generated by a single step extending the elastic element between the motors. For a linear spring, $F_K = F_1 = \ell K$. If both force scales of the single motor, F_s and F_d, are expressed as ratios to F_K, the two-motor parameters ϵ_2 and v_2 can be calculated as functions of the two dimensionless force ratios F_s/F_K and F_d/K_K, from which one can identify four different transport regimes [7]: when both force ratios are large, the coupling is weak and neither velocity nor unbinding rate is strongly affected by the coupling, i.e., $v_2 \approx v_1$ and $\epsilon_2 \approx 2\epsilon_1$ as for noninteracting motors (weak coupling regime). In the opposite limit, for which both force ratios are small, the coupling is strong, the velocity is reduced, and unbinding is enhanced (strong coupling regime). Furthermore, the motor pairs

exhibit two additional regimes, in which one of the two quantities is affected by coupling, while the other is not: A reduced velocity regime, in which the velocity is reduced, but the unbinding rate is (almost) unaffected by the strain force, is found for large F_d/F_K and small F_s/F_K. In the opposite case, for small F_d/F_K and large F_s/F_K, we have the enhanced unbinding regime, with an increased unbinding rate and a velocity that is unaffected.

The crossover lines between these regimes depend also on the dynamic parameters v_1 and ϵ_1, because the force between the motors is built up dynamically by stepping. They can be understood based on the comparison of three timescales: the times to build up forces comparable to the stall force and the detachment force and time for spontaneous unbinding of a motor [7, 8]. If the time for spontaneous unbinding is the shortest, there is no time to build up a sufficiently large strain force to affect the motors' behavior, corresponding to the weak coupling regime. If one of the other two timescales (or both) is shorter than the time for spontaneous unbinding, the corresponding parameter (ϵ_2, v_2 or both) is affected, resulting in the enhanced unbinding regime, the reduced velocity regime, or the strong coupling regime, respectively. We note that the presence of an external load force will provide an additional force scale, the external force itself, and additional timescales, such as the time it takes to equilibrate the distribution of the external force among the motors (force sharing).

Interestingly, which of the four regimes are accessed via a variation of the coupling strength is dependent on the motor species under consideration, because the force scales are characteristic parameters of these motors. For example, kinesin-1 motors are predicted to exhibit the strong and weak coupling regimes and, for intermediate coupling strength, the enhanced unbinding regime, while myosin V motors are predicted to be in the reduced velocity regime for intermediate couplings (in addition to also exhibiting the strong and weak coupling regimes) [7, 8]. This theoretical prediction was confirmed by experimental results: a pair of kinesin-1 motors was found to exhibit enhanced unbinding and little reduction of the velocity [79], while a reduced velocity was recently found for a pair of myosin V motors [66].

3.5 Open Questions

The cooperation of several molecular motor, specifically of well-defined small numbers of motors, is currently under intense investigation, mostly driven by new experimental techniques to couple molecular motors in a defined fashion, e.g., [25, 79]. These experiments address various aspects on different length scales, from molecular deformations on the scale of nanometers arising from elastic coupling-induced strains to increases in run lengths on the scale of many microns. These new experiments can be expected to lead to a rather detailed picture of motor cooperation in the near future, which will allow to address more detailed issues theoretically and to go beyond the coarse-grained descriptions of the motor configurations used so far. For example, we expect that precise empirical force dependencies of velocities and unbinding rates for a specific system can be used instead of the generic relations with

simple functional forms as employed in current studies. These improvements will, however, require fruitful interplay between model construction and experiments. One aspect that we hope can be addressed quite soon is the coupling to the chemistry of the motors, i.e. the interplay of nucleotide concentrations and forces in affecting the transport parameters of cooperatively pulled cargos. First steps in this direction have already been made, both from the experimental [96] and the theoretical sides [8, 49].

A key question will be what additional components are needed for certain patterns of movements. From the biochemical perspective, this is a question about additional molecular players such as regulatory components or proteins that modulate certain properties of the motors. Examples include the dynactin complex, which increases dynein's processivity and has been proposed as a candidate for regulating the interplay between kinesin and dynein motors [94], and the recently characterized regulators of dynein, NudE, and LIS1 [69]. From a theoretical perspective (where one tries to explain properties of a larger scale system, such as a complex of multiple motors, based on the known properties of its components, here the individual motors), these regulators modulate the parameters of the individual motors or of their coupling, so the question for regulatory factors can be addressed by studying the dynamic variation of parameters to explain observations that cannot be explained by fixed parameters characterizing the (unregulated) motors. For example, how would additional biochemical coordination have to affect a tug-of-war situation to result in the very long pauses that have been observed [55] or in directional memory after forced unbinding [59]. One example, in which such an extension of a tug-of-war is understood is the transport of early endosomes in the fungus *Ustilago maydis*, where a tug-of-war is controlled by the reversible binding and unbinding of a dynein motor to the moving cargo [83].

In order to understand transport in cells, it will also be necessary to consider the movements of motors on multiple levels of complexity (in addition to the different time and length scales discussed above). If single motors in vitro are considered as relatively simple systems,[7] complexity will increase and the space of possible dynamic behaviors extended by coupling motors in a defined way. These systems however are still relatively simple with respect to the number of different molecular components, which is relatively small. Moreover, all of these components are known. The system complexity increases further as one goes beyond the defined in vitro motility to movements in cell extracts and, finally, transport in vivo [4, 14]. Here, additional molecular players may modulate the properties of the motors and the possible existence of unknown components or of cross-talk and unknown interactions with other systems cannot easily be excluded. In this regard, theory can play an important role by bridging not only between different length and timescales but also between the different levels of complexity.

[7] Of course, the molecules themselves may also add a layer of complexity to the patterns of movements, for example if the motor has several different functional modes, as reported for dyneins [92].

References

1. Ali, M.Y., Kennedy, G.G., Safer, D., Trybus, K.M., Sweeney, H.L., Warshaw, D.M.: Myosin Va and myosin VI coordinate their steps while engaged in an in vitro tug of war during cargo transport. Proc Natl Acad Sci U S A **108**, E 535–541 (2011).
2. Ali, M.Y., Krementsova, E.B., Kennedy, G.G., Mahaffy, R., Pollard, T.D., Trybus, K.M., Warshaw, D.M.: Myosin va maneuvers through actin intersections and diffuses along microtubules. Proc Natl Acad Sci U S A **104**, 4332–6 (2007).
3. Atzberger, P.J., Peskin, C.S.: A brownian dynamics model of kinesin in three dimensions incorporating the force-extension profile of the coiled-coil cargo tether. Bull Math Biol **68**, 131–60 (2006).
4. Barak, P., Rai, A., Rai, P., Mallik, R.: Quantitative optical trapping on single organelles in cell extract. Nat Methods **10**, 68–70 (2013).
5. Beeg, J., Klumpp, S., Dimova, R., Gracià, R.S., Unger, E., Lipowsky, R.: Transport of beads by several kinesin motors. Biophys J **94**, 532–41 (2008).
6. Bell, G.I.: Models for the specific adhesion of cells to cells. Science **200**, 618–627 (1978).
7. Berger, F., Keller, C., Klumpp, S., Lipowsky, R.: Distinct transport regimes of two elastically coupled molecular motors. Phys Rev Lett **108**, 208101 (2012).
8. Berger, F., Keller, C., Lipowsky, R., Klumpp, S.: Elastic coupling effects in cooperative transport by a pair of molecular motors. Cell Molec Bioeng **6**, 48–64 (2013).
9. Berger, F., Keller, C., Müller, M.J.I., Klumpp, S., Lipowsky, R.: Co-operative transport by molecular motors. Biochem Soc Trans **39**, 1211–5 (2011).
10. Berger, F., Müller, M.J.I., Lipowsky, R.: Enhancement of the processivity of kinesin-transported cargo by myosin V. Europhys Lett **87**, 28,002 (2009).
11. Bieling, P., Telley, I.A., Piehler, J., Surrey, T.: Processive kinesins require loose mechanical coupling for efficient collective motility. EMBO Rep **9**, 1121–7 (2008).
12. Bierbaum, V., Lipowsky, R.: Chemomechanical coupling and motor cycles of myosin V. Biophys J **100**, 1747–55 (2011).
13. Bierbaum, V., Lipowsky, R.: Dwell time distributions of the molecular motor myosin v. PLoS One **8**, e55366 (2013).
14. Blehm, B.H., Schroer, T.A., Trybus, K.M., Chemla, Y.R., Selvin, P.R.: In vivo optical trapping indicates kinesin's stall force is reduced by dynein during intracellular transport. Proc Natl Acad Sci U S A **110**, 3381–6 (2013).
15. Block, S.M.: Kinesin motor mechanics: Binding, stepping, tracking, gating, and limping. Biophys J **92**, 2986–95 (2007).
16. Böhm, K.J., Stracke, R., Mühlig, P., Unger, E.: Motor protein-driven unidirectional transport of micrometer-sized cargoes across isopolar microtubule arrays. Nanotechnology **12**, 238–244 (2001).
17. Bouzat, S., Falo, F.: The influence of direct motor-motor interaction in models for cargo transport by a single team of motors. Phys Biol **7**, 046009 (2010).
18. Campàs, O., Kafri, Y., Zeldovich, K.B., Casademunt, J., Joanny, J.F.: Collective dynamics of interacting molecular motors. Phys Rev Lett **97**, 038101 (2006).
19. Carter, N.J., Cross, R.A.: Mechanics of the kinesin step. Nature **435**, 308–12 (2005).
20. Clancy B.E., Behnke-Parks W.M., Andreasson J.O.L., Rosenfeld S.S., Block S.M.: A universal pathway for kinesin stepping. Nature Struct. Mol. Biol. **18** 1020–7 (2011).
21. Clemen, A.E.M., Vilfan, M., Jaud, J., Zhang, J., Bärmann, M., Rief, M.: Force-dependent stepping kinetics of myosin-V. Biophys J **88**, 4402–10 (2005).
22. Constantinou, P.E., Diehl, M.R.: The mechanochemistry of integrated motor protein complexes. J Biomech **43**, 31–7 (2010).
23. Coppin, C., Pierce, D., Hsu, L., Vale, R.: The load dependence of kinesin's mechanical cycle. Proc Natl Acad Sci U S A **94**, 8539–8544 (1997).
24. Crevenna, A.H., Madathil, S., Cohen, D.N., Wagenbach, M., Fahmy, K., Howard, J.: Secondary structure and compliance of a predicted flexible domain in kinesin-1 necessary for cooperation of motors. Biophys J **95**, 5216–27 (2008).

25. Derr, N.D., Goodman, B.S., Jungmann, R., Leschziner, A.E., Shih, W.M., Reck-Peterson, S.L.: Tug-of-war in motor protein ensembles revealed with a programmable dna origami scaffold. Science **338**, 662–5 (2012).
26. Driver, J.W., Jamison, D.K., Uppulury, K., Rogers, A.R., Kolomeisky, A.B., Diehl, M.R.: Productive cooperation among processive motors depends inversely on their mechanochemical efficiency. Biophys J **101**, 386–95 (2011).
27. Driver, J.W., Rogers, A.R., Jamison, D.K., Das, R.K., Kolomeisky, A.B., Diehl, M.R.: Coupling between motor proteins determines dynamic behaviors of motor protein assemblies. Phys Chem Chem Phys **12**, 10,398–405 (2010).
28. Erickson, R.P., Jia, Z., Gross, S.P., Yu, C.C.: How molecular motors are arranged on a cargo is important for vesicular transport. PLoS Comput Biol **7**, e1002,032 (2011).
29. Fisher, M.E., Kolomeisky, A.B.: Simple mechanochemistry describes the dynamics of kinesin molecules. Proc Natl Acad Sci USA **98**, 7748–7753 (2001).
30. Furuta, K., Furuta, A., Toyoshima, Y.Y., Amino, M., Oiwa, K., Kojima, H.: Measuring collective transport by defined numbers of processive and nonprocessive kinesin motors. Proc Natl Acad Sci U S A **110**, 501–6 (2013).
31. Gagliano, J., Walb, M., Blaker, B., Macosko, J.C., Holzwarth, G.: Kinesin velocity increases with the number of motors pulling against viscoelastic drag. Eur Biophys J **39**, 801–13 (2010).
32. Gennerich, A., Carter, A.P., Reck-Peterson, S.L., Vale, R.D.: Force-induced bidirectional stepping of cytoplasmic dynein. Cell **131**, 952 (2007).
33. Grant, B.J., Gheorghe, D.M., Zheng, W., Alonso, M., Huber, G., Dlugosz, M., McCammon, J.A., Cross, R.A.: Electrostatically biased binding of kinesin to microtubules. PLoS Biol **9**, e1001207 (2011).
34. Gross, S.P., Vershinin, M., Shubeita, G.T.: Cargo transport: two motors are sometimes better than one. Curr Biol **17**, R478–86 (2007).
35. Hancock, W.O., Howard, J.: Kinesin's processivity results from mechanical and chemical coordination between the ATP hydrolysis cycles of the two motor domains. Proc Natl Acad Sci USA **96**, 13147–13152 (1999).
36. Hendricks, A.G., Perlson, E., Ross, J.L., Schroeder 3rd, H.W., Tokito, M., Holzbaur, E.L.F.: Motor coordination via a tug-of-war mechanism drives bidirectional vesicle transport. Curr Biol **20**, 697–702 (2010).
37. Hill, T.: Free Energy Transduction in Biology. Academic Press, New York (1977).
38. Hill, T.L.: Interrelations between random walks on diagrams (graphs) with and without cycles. Proc Natl Acad Sci USA **85**, 2879–2883 (1988).
39. Hill, T.L.: Number of visits to a state in a random walk, before absorption, and related topics. Proc Natl Acad Sci USA **85**, 4577–4581 (1988).
40. Holmes, K.C.: Muscle contraction. In: L. Wolpert (ed.) The limits of reductionism in biology, Novartis Foundation Symposium **213**, pp. 76–92. Wiley, Chichester (1998).
41. Howard, J.: Mechanics of Motor Proteins and the Cytoskeleton. Sinauer Associates, Sunderland (Mass.) (2001).
42. Howard, J., Hudspeth, A.J., Vale, R.D.: Movement of microtubules by single kinesin molecules. Nature **342**, 154–158 (1989).
43. Hwang, W., Lang, M.J., Karplus, M.: Force generation in kinesin hinges on cover-neck bundle formation. Structure **16**, 62–71 (2008).
44. Hyeon, C., Klumpp, S., Onuchic, J.N.: Kinesin's backsteps under mechanical load. Phys Chem Chem Phys **11**, 4899–910 (2009).
45. Hyeon, C., Onuchic, J.N.: Mechanical control of the directional stepping dynamics of the kinesin motor. Proc Natl Acad Sci U S A **104**, 17,382–7 (2007).
46. Jülicher, F., Ajdari, A., Prost, J.: Modeling molecular motors. Rev Mod Phys **69**, 1269–1281 (1997).
47. Keller, C.: Coupled molecular motors. Diploma thesis, Humboldt-Universität, Berlin (2009).
48. Keller, C.: Coupled Molecular Motors: Network Representation & Dynamics of Kinesin Motor Pairs. Ph.D. thesis, Universität Potsdam (2013).

49. Keller, C., Berger, F., Liepelt, S., Lipowsky, R.: Network complexity and parametric simplicity for cargo transport by two molecular motors. J Stat Phys **150**, 205–234 (2013).
50. King, S.J., Schroer, T.A.: Dynactin increases the processivity of the cytoplasmic dynein motor. Nat Cell Biol **2**, 20 (2000).
51. Klumpp, S., Lipowsky, R.: Cooperative cargo transport by several molecular motors. Proc Natl Acad Sci U S A **102**, 17,284–9 (2005).
52. Korn, C.B., Klumpp, S., Lipowsky, R., Schwarz, U.S.: Stochastic simulations of cargo transport by processive molecular motors. J Chem Phys **131**, 245,107 (2009).
53. Kramers, H.: Brownian motion in a field of force and the diffusion model of chemical reactions. Physica **7**, 284 (1940).
54. Kunwar, A., Mogilner, A.: Robust transport by multiple motors with nonlinear force-velocity relations and stochastic load sharing. Phys Biol **7**, 16012 (2010).
55. Kunwar, A., Tripathy, S.K., Xu, J., Mattson, M.K., Anand, P., Sigua, R., Vershinin, M., McKenney, R.J., Yu, C.C., Mogilner, A., Gross, S.P.: Mechanical stochastic tug-of-war models cannot explain bidirectional lipid-droplet transport. Proc Natl Acad Sci U S A **108**, 18960–5 (2011).
56. Larson, A.G., Landahl, E.C., Rice, S.E.: Mechanism of cooperative behaviour in systems of slow and fast molecular motors. Phys Chem Chem Phys **11**, 4890–8 (2009).
57. Leduc, C., Campàs, O., Zeldovich, K.B., Roux, A., Jolimaitre, P., Bourel-Bonnet, L., Goud, B., Joanny, J.F., Bassereau, P., Prost, J.: Cooperative extraction of membrane nanotubes by molecular motors. Proc Natl Acad Sci USA **101**, 17096–17101 (2004).
58. Leduc, C., Ruhnow, F., Howard, J., Diez, S.: Detection of fractional steps in cargo movement by the collective operation of kinesin-1 motors. Proc Natl Acad Sci USA **104**, 10847–10852 (2007).
59. Leidel, C., Longoria, R.A., Gutierrez, F.M., Shubeita, G.T.: Measuring molecular motor forces in vivo: implications for tug-of-war models of bidirectional transport. Biophys J **103**, 492–500 (2012).
60. Li, X., Lipowsky, R., Kierfeld, J.: Critical motor number for fractional steps of cytoskeletal filaments in gliding assays. PLoS One **7**, e43219 (2012).
61. Liepelt, S., Lipowsky, R.: Kinesin's network of chemomechanical motor cycles. Phys Rev Lett **98**, 258102 (2007).
62. Liepelt, S., Lipowsky, R.: Steady-state balance conditions for molecular motor cycles and stochastic nonequilibrium processes. Europhys Lett **77**, 50002 (2007).
63. Liepelt, S., Lipowsky, R.: Impact of slip cycles on the operation modes and efficiency of molecular motors. J Stat Phys **141**, 1–16 (2010).
64. Lipowsky, R., Klumpp, S.: 'Life is motion' - multiscale motility of molecular motors. Physica A **352**, 53–112 (2005).
65. Lipowsky, R., Liepelt, S.: Chemomechanical coupling of molecular motors: Thermodynamics, network representations and balanced conditions. J Stat Phys 130, 39–67 (2008). Erratum: J Stat Phys **135**, 777–778 (2009).
66. Lu, H., Efremov, A.K., Bookwalter, C.S., Krementsova, E.B., Driver, J.W., Trybus, K.M., Diehl, M.R.: Collective dynamics of elastically coupled myosin V motors. J Biol Chem **287**, 27,753–61 (2012).
67. Mallik, R., Carter, B.C., Lex, S.A., King, S.J., Gross, S.: Cytoplasmic dynein functions as a gear in response to load. Nature **427**, 649 (2004).
68. Mallik, R., Petrov, D., Lex, S.A., King, S., Gross, S.: Building complexity: An in vitro study of cytoplasmic dynein with in vivo implications. Curr Biol **15**, 2075–2085 (2005).
69. McKenney, R.J., Vershinin, M., Kunwar, A., Vallee, R.B., Gross, S.P.: Lis1 and NudE induce a persistent dynein force-producing state. Cell **141**, 304–14 (2010).
70. Mehta, A.D., Rock, R.S., Rief, M., Spudich, J.A., Mooseker, M.S., Cheney, R.E.: Myosin-V is a processive actin-based motor. Nature **400**, 590–593 (1999).
71. Müller, M.J.I., Klumpp, S., Lipowsky, R.: Motility states of molecular motors engaged in a stochastic tug-of-war. J Stat Phys **133**, 1059–1081 (2008).

72. Müller, M.J.I., Klumpp, S., Lipowsky, R.: Tug-of-war as a cooperative mechanism for bidirectional cargo transport by molecular motors. Proc Natl Acad Sci USA **105**, 4609–4614 (2008).
73. Müller, M.J.I., Klumpp, S., Lipowsky, R.: Bidirectional transport by molecular motors: enhanced processivity and response to external forces. Biophys J **98**, 2610–8 (2010).
74. Ökten, Z., Churchman, L.S., Rock, R.S., Spudich, J.A.: Myosin VI walks hand-over-hand along actin. Nat Struct Mol Biol **11**, 884 (2004).
75. Posta, F., D'Orsogna, M.R., Chou, T.: Enhancement of cargo processivity by cooperating molecular motors. Phys Chem Chem Phys **11**, 4851–60 (2009).
76. Rice, S., Lin, A.W., Safer, D., Hart, C.L., Naber, N., Carragher, B.O., Cain, S.M., Pechatnikova, E., Wilson-Kubalek, E.M., Whittaker, M., Pate, E., Cooke, R., Taylor, E.W., Milligan, R.A., Vale, R.D.: A structural change in the kinesin motor protein that drives motility. Nature **402**, 778–84 (1999).
77. Risken, H.: The Fokker-Planck Equation. Springer, Berlin Heidelberg (1996).
78. Rock, R.S., Rice, S.E., Wells, A.L., Purcell, T.J., Spudich, J.A., Sweeney, H.L.: Myosin VI is a processive motor with a large step size. Proc Natl Acad Sci USA **98**, 13,655 (2001).
79. Rogers, A.R., Driver, J.W., Constantinou, P.E., Kenneth Jamison, D., Diehl, M.R.: Negative interference dominates collective transport of kinesin motors in the absence of load. Phys Chem Chem Phys **11**, 4882–9 (2009).
80. Romberg, L., Vale, R.: Chemomechanical cycle of kinesin differs from that of myosin. Nature **361**, 168–170 (1993).
81. Schliwa, M., Woehlke, G.: Molecular motors. Nature **422**, 759–765 (2003).
82. Schnitzer, M.J., Visscher, K., Block, S.M.: Force production by single kinesin motors. Nature Cell Biol. **2**, 718–723 (2000).
83. Schuster, M., Lipowsky, R., Assmann, M.A., Lenz, P., Steinberg, G.: Transient binding of dynein controls bidirectional long-range motility of early endosomes. Proc Natl Acad Sci U S A **108**, 3618–23 (2011).
84. Soppina, V., Rai, A.K., Ramaiya, A.J., Barak, P., Mallik, R.: Tug-of-war between dissimilar teams of microtubule motors regulates transport and fission of endosomes. Proc Natl Acad Sci U S A **106**, 19,381–6 (2009).
85. Svoboda, K., Block, S.M.: Force and velocity measured for single kinesin molecules. Cell **77**, 773 (1994).
86. Svoboda, K., Schmidt, C.F., Schnapp, B.J., Block, S.M.: Direct observation of kinesin stepping by optical trapping interferometry. Nature **365**, 721–727 (1993).
87. Toba, S., Watanabe, T.M., Yamaguchi-Okimoto, L., Toyoshima, Y.Y., Higuchi, H.: Overlapping hand-over-hand mechanism of single molecular motility of cytoplasmic dynein. Proc Natl Acad Sci USA **103**, 5741 (2006).
88. van Kampen, N.: Stochastic Processes in Physics and Chemistry. Elsevier, Amsterdam (1992).
89. Veigel, C., Coluccio, L.M., Jontes, J.D., Sparrow, J.C., Milligan, R.D., Molloy, J.E.: The motor protein myosin-I produces its working stroke in two steps. Nature **398**, 530–533 (1999).
90. Vershinin, M., Carter, B.C., Razafsky, D.S., King, S.J., Gross, S.P.: Multiple-motor based transport and its regulation by tau. Proc Natl Acad Sci U S A **104**, 87–92 (2007).
91. Visscher, K., Schnitzer, M.J., Block, S.M.: Single kinesin molecules studied with a molecular force clamp. Nature **400**, 184 (1999).
92. Walter, W.J., Koonce, M.P., Brenner, B., Steffen, W.: Two independent switches regulate cytoplasmic dynein's processivity and directionality. Proc Natl Acad Sci U S A **109**, 5289–93 (2012).
93. Wang, Z., Li, M.: Force-velocity relations for multiple-molecular-motor transport. Phys Rev E **80**, 041923 (2009).
94. Welte, M.A.: Bidirectional transport along microtubules. Curr Biol **14**, R525–37 (2004).
95. Welte, M.A., Gross, S.P.: Molecular motors: a traffic cop within? HFSP J **2**, 178–82 (2008).
96. Xu, J., Shu, Z., King, S.J., Gross, S.P.: Tuning multiple motor travel via single motor velocity. Traffic **13**, 1198–205 (2012).

97. Yildiz, A., Forkey, J.N., McKinney, S.A., Ha, T., Goldman, Y.E., Selvin, P.R.: Myosin V walks hand-over-hand: Single fluorophore imaging with 1.5-nm localization. Science **300**, 2061–2065 (2003).
98. Yildiz, A., Selvin, P.R.: Fluorescence imaging with one nanometer accuracy: application to molecular motors. Acc Chem Res **38**, 574–82 (2005).
99. Yildiz, A., Tomishige, M., Gennerich, A., Vale, R.D.: Intramolecular strain coordinates kinesin stepping behaviour along microtubules. Cell **134**, 1030–1040 (2008).
100. Yildiz, A., Tomishige, M., Vale, R.D., Selvin, P.R.: Kinesin walks hand-over-hand. Science **303**, 676–678 (2004).
101. Zhang, Y.: Cargo transport by several motors. Phys Rev E **83**, 011909 (2011).